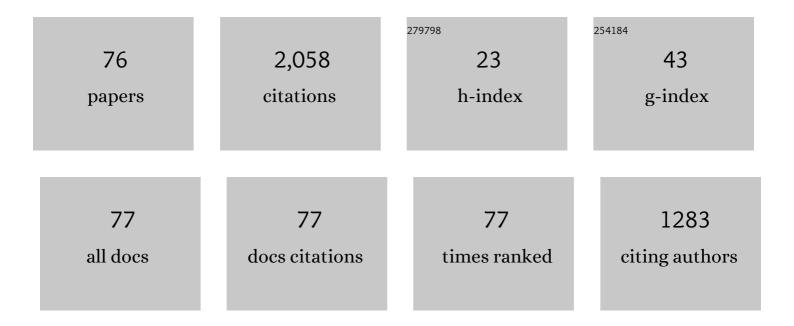
## **Dmitry Rudakov**

List of Publications by Year in descending order

Source: https://exaly.com/author-pdf/4916967/publications.pdf Version: 2024-02-01



#	Article	IF	CITATIONS
1	Transport by intermittent convection in the boundary of the DIII-D tokamak. Physics of Plasmas, 2001, 8, 4826-4833.	1.9	322
2	Dust in magnetic fusion devices. Plasma Physics and Controlled Fusion, 2011, 53, 083001.	2.1	158
3	Far SOL transport and main wall plasma interaction in DIII-D. Nuclear Fusion, 2005, 45, 1589-1599.	3.5	123
4	Control and dissipation of runaway electron beams created during rapid shutdown experiments in DIII-D. Nuclear Fusion, 2013, 53, 083004.	3.5	96
5	Edge-localized mode dynamics and transport in the scrape-off layer of the DIII-D tokamak. Physics of Plasmas, 2005, 12, 072516.	1.9	66
6	Recent progress in understanding the behavior of dust in fusion devices. Plasma Physics and Controlled Fusion, 2008, 50, 124054.	2.1	66
7	Interpretive modeling of simple-as-possible-plasma discharges on DIII-D using the OEDGE code. Journal of Nuclear Materials, 2003, 313-316, 883-887.	2.7	65
8	Spectroscopic measurement of atomic and molecular deuterium fluxes in the DIII-D plasma edge. Plasma Physics and Controlled Fusion, 2006, 48, 1165-1180.	2.1	58
9	Measurement of runaway electron energy distribution function during high-Z gas injection into	1.9	50
10	The inter-ELM tungsten erosion profile in DIII-D H-mode discharges and benchmarking with ERO+OEDGE modeling. Nuclear Fusion, 2017, 57, 056034.	3.5	47
11	Arcing and its role in PFC erosion and dust production in DIII-D. Journal of Nuclear Materials, 2013, 438, S805-S808.	2.7	42
12	Simulation of gross and net erosion of high-Z materials in the DIII-D divertor. Nuclear Fusion, 2016, 56, 016021.	3.5	41
13	The magnitude of plasma flux to the main-wall in the DIII-D tokamak. Plasma Physics and Controlled Fusion, 2005, 47, 1579-1607.	2.1	40
14	13C transport studies in L-mode divertor plasmas on DIII-D. Journal of Nuclear Materials, 2005, 337-339, 30-34.	2.7	38
15	Fast imaging of edge localized mode structure and dynamics in DIII-D. Physics of Plasmas, 2008, 15, 032504.	1.9	38
16	Intrinsic rotation generation in ELM-free H-mode plasmas in the DIII-D tokamak—Experimental observations. Physics of Plasmas, 2011, 18, .	1.9	35
17	Exposures of tungsten nanostructures to divertor plasmas in DIII-D. Physica Scripta, 2016, T167, 014055.	2.5	29
18	DIVIMP modeling of the toroidally symmetrical injection of 13CH4 into the upper SOL of DIII-D. Journal of Nuclear Materials, 2005, 337-339, 124-128.	2.7	27

#	Article	IF	CITATIONS
19	Poloidally and radially resolved parallel D+ velocity measurements in the DIII-D boundary and comparison to neoclassical computations. Physics of Plasmas, 2011, 18, 032510.	1.9	27
20	Observations of wall conditioning by means of boron powder injection in DIII-D H-mode plasmas. Nuclear Fusion, 2020, 60, 126010.	3.5	27
21	Analysis of a tungsten sputtering experiment in DIII-D and code/data validation of high redeposition/reduced erosion. Fusion Engineering and Design, 2015, 94, 67-71.	1.9	25
22	Tungsten erosion by unipolar arcing in DIII-D. Physica Scripta, 2017, T170, 014034.	2.5	25
23	OEDGE modeling of 13C deposition in the inner divertor of DIII-D. Journal of Nuclear Materials, 2005, 337-339, 79-83.	2.7	24
24	Fast camera imaging of dust in the DIII-D tokamak. Journal of Nuclear Materials, 2009, 390-391, 216-219.	2.7	24
25	Net versus gross erosion of high- <i>Z</i> materials in the divertor of DIII-D. Physica Scripta, 2014, T159, 014030.	2.5	23
26	An experimental comparison of gross and net erosion of Mo in the DIII-D divertor. Journal of Nuclear Materials, 2013, 438, S309-S312.	2.7	22
27	Experimental validation of a model for particle recycling and tungsten erosion during ELMs in the DIII-D divertor. Nuclear Materials and Energy, 2018, 17, 164-173.	1.3	22
28	Overview of the recent DiMES and MiMES experiments in DIII-D. Physica Scripta, 2009, T138, 014007.	2.5	20
29	Measurements of net erosion and redeposition of molybdenum in DIII-D. Journal of Nuclear Materials, 2013, 438, S822-S826.	2.7	20
30	Study of argon expulsion from the post-disruption runaway electron plateau following low-Z massive gas injection in DIII-D. Physics of Plasmas, 2020, 27, .	1.9	20
31	Impact of ELM control techniques on tungsten sputtering in the DIII-D divertor and extrapolations to ITER. Physics of Plasmas, 2019, 26, .	1.9	19
32	Evidence of near-SOL tungsten accumulation using a far-SOL collector probe array and OEDGE modelling in the DIII-D metal rings L-mode discharges. Nuclear Materials and Energy, 2019, 19, 287-294.	1.3	19
33	DiMES PMI research at DIII-D in support of ITER and beyond. Fusion Engineering and Design, 2017, 124, 196-201.	1.9	18
34	Utilization of outer-midplane collector probes with isotopically enriched tungsten tracer particles for impurity transport studies in the scrape-off layer of DIII-D (invited). Review of Scientific Instruments, 2018, 89, 10I115.	1.3	18
35	OEDGE modeling of the DIII-D H-mode 13CH4 puffing experiment. Journal of Nuclear Materials, 2007, 363-365, 140-145.	2.7	17
36	Advances in understanding of high- <i>Z</i> material erosion and re-deposition in low- <i>Z</i> wall environment in DIII-D. Nuclear Fusion, 2017, 57, 056016.	3.5	16

#	Article	IF	CITATIONS
37	Study of Z scaling of runaway electron plateau final loss energy deposition into wall of DIII-D. Physics of Plasmas, 2017, 24, .	1.9	16
38	A review of direct experimental measurements of detachment. Plasma Physics and Controlled Fusion, 2018, 60, 044008.	2.1	16
39	Evaluation of silicon carbide as a divertor armor material in DIII-D H-mode discharges. Nuclear Fusion, 2021, 61, 066005.	3.5	16
40	Far scrape-off layer and near wall plasma studies in DIII-D. Journal of Nuclear Materials, 2005, 337-339, 717-721.	2.7	15
41	Study of argon assimilation into the post-disruption runaway electron plateau in DIII-D and comparison with a 1D diffusion model. Nuclear Fusion, 2019, 59, 106014.	3.5	14
42	Experiments to measure hydrogen release from graphite walls during disruptions in DIII-D. Journal of Nuclear Materials, 2009, 390-391, 597-601.	2.7	13
43	Use of isotopic tungsten tracers and a stable-isotope-mixing model to characterize divertor source location in the DIII-D metal rings campaign. Nuclear Materials and Energy, 2019, 19, 358-363.	1.3	13
44	ERO modeling and analysis of tungsten erosion and migration from a toroidally symmetric source in the DIII-D divertor. Nuclear Fusion, 2020, 60, 016018.	3.5	13
45	Localized divertor leakage measurements using isotopic tungsten sources during edge-localized mode-y H-mode discharges on DIII-D. Nuclear Fusion, 2020, 60, 016028.	3.5	13
46	Modeling of ExB effects on tungsten re-deposition and transport in the DIII-D divertor. Nuclear Fusion, 2021, 61, 096018.	3.5	13
47	Particle flux and radial profiles in the SOL of DIII-D during ELMing H-mode. Journal of Nuclear Materials, 2007, 363-365, 1066-1070.	2.7	12
48	Atomic insight into concurrent He, D, and T sputtering and near-surface implantation of 3C-SiC crystallographic surfaces. Nuclear Materials and Energy, 2019, 19, 1-6.	1.3	12
49	Transport of tungsten to collector probes in DIII-D. Nuclear Materials and Energy, 2019, 18, 87-92.	1.3	12
50	The effect of thermo-oxidation on plasma performance and in-vessel components in DIII-D. Nuclear Fusion, 2013, 53, 073008.	3.5	11
51	Divertor and midplane materials evaluation system in DIII-D. Journal of Nuclear Materials, 2007, 363-365, 276-281.	2.7	10
52	OEDGE modeling for the planned tungsten ring experiment on DIII-D. Nuclear Materials and Energy, 2017, 12, 755-761.	1.3	10
53	Measurements of tungsten migration in the DIII-D divertor. Physica Scripta, 2017, T170, 014041.	2.5	10
54	3D modeling of boron transport in DIII-D L-mode wall conditioning experiments. Nuclear Materials and Energy, 2021, 26, 100900.	1.3	10

#	Article	IF	CITATIONS
55	Indications of an inward pinch in the inner SOL of DIII-D from 13C deposition experiments. Journal of Nuclear Materials, 2009, 390-391, 376-379.	2.7	9
56	Control of high-Z PFC erosion by local gas injection in DIII-D. Journal of Nuclear Materials, 2015, 463, 605-610.	2.7	9
57	Plasma interactions with the outboard chamber wall in DIII-D. Journal of Nuclear Materials, 2009, 390-391, 785-788.	2.7	8
58	Experimental verification of ion impact angle distribution at divertor surfaces using micro-engineered targets on DiMES at DIII-D. Nuclear Materials and Energy, 2021, 27, 100965.	1.3	7
59	Modeling, analysis, and code/data validation of DIII-D tokamak divertor experiments on ELM and non-ELM plasma tungsten sputtering erosion. Nuclear Fusion, 2020, 60, 126026.	3.5	7
60	Reduced model of high-Z impurity redeposition and erosion in tokamak divertor and its application to DIII-D experiments. Plasma Physics and Controlled Fusion, 2019, 61, 125015.	2.1	6
61	Reproduction of collector probe deposition profiles using the far-SOL impurity transport code 3DLIM. Nuclear Materials and Energy, 2020, 25, 100811.	1.3	6
62	The role of B <sub>T</sub> -dependent flows on W accumulation at the edge of the confined plasma. Nuclear Fusion, 2022, 62, 026037.	3.5	6
63	Developing solid-surface plasma facing components for pilot plants and reactors with replenishable wall claddings and continuous surface conditioning. Part A: concepts and questions. Plasma Physics and Controlled Fusion, 2022, 64, 055018.	2.1	6
64	Dynamic control of low-Z material deposition and tungsten erosion by strike point sweeping on DIII-D. Nuclear Materials and Energy, 2017, 12, 392-398.	1.3	5
65	Development of Surface Eroding Thermocouples in Small Angle Slot Divertor in DIII-D. IEEE Transactions on Plasma Science, 2020, 48, 1804-1809.	1.3	5
66	Modelling dust transport in DIII-D with DTOKS-Upgrade. Plasma Physics and Controlled Fusion, 2021, 63, 045002.	2.1	5
67	Net versus gross erosion of silicon carbide in DIII-D divertor. Physica Scripta, 2020, T171, 014064.	2.5	5
68	High-Z material erosion and its control in DIII-D carbon divertor. Nuclear Materials and Energy, 2017, 12, 247-252.	1.3	4
69	Robust impurity detection and tracking for tokamaks. Physical Review E, 2020, 102, 043311.	2.1	4
70	ELM and inter-ELM heat and particle flux to a secondary divertor in the DIII-D tokamak. Nuclear Fusion, 2021, 61, 086024.	3.5	4
71	Dust appearance rates during neutral beam injection and after oxygen bake in the DIII-D tokamak. Journal of Nuclear Materials, 2011, 415, S1102-S1105.	2.7	2
72	Quantification of chemical erosion in the DIII-D divertor and implications for ITER. Journal of Nuclear Materials, 2011, 415, S141-S144.	2.7	2

#	Article	IF	CITATIONS
73	A Method to Identify the Heat Flux From Photons and Neutrals at the Divertor Target. IEEE Transactions on Plasma Science, 2022, 50, 4257-4261.	1.3	1
74	Separatrix-to-Wall Simulations of Impurity Transport with a Fully Three-Dimensional Wall in DIII-D. Fusion Science and Technology, 2023, 79, 36-45.	1.1	1
75	Estimation of plasma ion saturation current and reduced tip arcing using Langmuir probe harmonics. Review of Scientific Instruments, 2017, 88, 033505.	1.3	ο
76	Developing solid-surface plasma facing components for pilot plants and reactors with replenishable wall claddings and continuous surface conditioning. Part B: required research in present tokamaks. Plasma Physics and Controlled Fusion, 2022, 64, 055003.	2.1	0